Radiation enhanced oxidation of proton-irradiated copper thin-films: Towards a new concept of ultra-high radiation dosimetry

Cite as: AIP Advances **9**, 085217 (2019); https://doi.org/10.1063/1.5096606
Submitted: 19 March 2019 . Accepted: 11 August 2019 . Published Online: 19 August 2019

Georgi Gorine, Giuseppe Pezzullo, Didier Bouvet, Federico Ravotti, and Jean-Michel Sallese

Radiation enhanced oxidation of proton-irradiated copper thin-films: Towards a new concept of ultra-high radiation dosimetry

Cite as: AIP Advances 9, 085217 (2019); doi: 10.1063/1.5096606
Submitted: 19 March 2019 • Accepted: 11 August 2019 •
Published Online: 19 August 2019

Georgi Gorine,[1,2,a)] Giuseppe Pezzullo,[1] Didier Bouvet,[3] Federico Ravotti,[1] and Jean-Michel Sallese[2]

AFFILIATIONS

[1]EP-DT-DD, European Organization for Nuclear Research (CERN), 1211 Geneva, Switzerland
[2]EDLAB, École Polytechnique Fédérale de Lausanne (EPFL), 1015 Lausanne, Switzerland
[3]CMi, École Polytechnique Fédérale de Lausanne (EPFL), 1015 Lausanne, Switzerland

[a)]**Electronic mail:** georgi.gorine@cern.ch; ggorine@gmail.com

ABSTRACT

The effects of extreme radiation levels on the electrical resistivity of metal thin films made of copper were studied by means of electrical measurements and post irradiation imaging. Different 3x3 mm^2 chips were produced by depositing 500 nm of meander shaped copper on top of a silicon substrate. A subset of samples was also passivated by sputtering 300 nm of SiO_2. During irradiation with 23 GeV protons up to 1.2 x 10^{17} p/cm^2 at the CERN IRRAD Proton Facility, only not-passivated copper samples have shown an increase of resistivity proportional to the particle fluence, indicating that the dominant factor of the resistivity increase is not directly an accumulation of displacement damage, but the radiation enhanced oxidation of the copper film exposed to air. Post-irradiation imaging of the chips cross sections has confirmed the presence of a grown copper oxide film on the surface as well as oxide wells that extended within the bulk following the grain boundaries. This permanent increase of resistance due to radiation enhanced oxidation, can be used for monitoring high energy particles fluence up to levels currently not reachable by standard silicon technology.

I. INTRODUCTION

The effects of radiation on metals have been considered in a number of studies aimed to understand and predict radiation-induced degradation of materials and components used in nuclear reactors as well as in high-energy physics experiments.[1,2] Several property variations were reported like: changes in the material stiffness, generation of internal voids, surface swelling, as well as changes in the electrical resistivity of the irradiated metal and/or alloy.[3] In the latter, a qualitative trend in increasing copper resistivity was observed, explained as result of transmutations (e.g. decay of ^{64}Cu into ^{64}Zn and ^{64}Ni by beta emission), and defects generation in the lattice due to displacement damage.[4] Such experiments were carried out on relatively thick metal samples (several mm thickness), and not on thin-film samples of sub-μm size, where the effects of very high fluences of energetic particles (>10^{20} p/cm^2), to the best of our knowledge, have never been studied in detail.

In this work, we analyze and explain the effects of radiation on 500 nm thin copper layers, by direct electrical characterization before, during, and after irradiation, as well as by morphological observations combining Focused Ion Beam (FIB) milling with Scanning Electron Microscopy (SEM).

This paper is structured as follows. Section II provides a review on the radiation effects on metals, followed by a description of the irradiation tests already performed within this study on metal thin-films of copper, chromium and aluminum. Section III, illustrates the experimental methods used in this project, and provides a description of the IRRAD proton facility, where the irradiation was

performed. To explain the phenomenological observations resulted from the electrical and SEM-FIB analysis, a model for radiation enhanced oxidation is proposed and discussed in Section IV. Finally, Section V, presents the design guidelines and possible applications of the presented findings such as technology for monitoring very high radiation levels.

II. THEORY

A. Radiation damage in metals

Radiation is known to cause significant changes in the physical and mechanical properties of materials due to energy released by ionization (direct or indirect), and/or by elastic collisions (primary knock-on atom) that initiate atomic displacement cascades. Ionizing radiation, commonly expressed as absorbed energy per unit of mass, or Gy (1 Gray = 1 J/Kg), can lead to radiolysis and free radical production responsible of chemical bonds damages in organic molecules. Instead in metals, ionizing radiation does not induce any permanent effect, since the released energy generates only a transient effect in which the stripped electron (ionized) gets immediately replaced by another free-electron available in the conduction band of the metal.[5] Contrarily, the non-ionizing energy transfer of recoil energy by direct interaction with the metallic atom, can produce microstructural changes in the crystal lattice in form of defects (vacancies and interstitials), phase transitions, and transmutations.[6–8] The release of non-ionizing energy is quantified by means of displacements per atom (dpa) which represents the number of atoms displaced from their normal lattice sites as a result of a given number of bombarding particles, or particle fluence Φ (p/cm^2).

B. Radiation dependent resistors

Current silicon-based radiation monitoring devices cannot measure very high radiation levels. For example at CERN, in the LHC and its experiments, RadFETs (radiation dependent transistors) can measure up to 100 kGy doses, and *p-i-n* diodes withstand up to 10^{15} p/cm^2 particle fluence.[9] Such levels are orders of magnitude less then the radiation levels expected in future CERN experiments, like the Future Circular Collider (FCC)[10] with simulated doses of tens of MGy and >10^{17} p/cm^2 particle fluence.[11]

In order to overcome these limitations of silicon devices, we have focused our research on a new dosimetry concept based on the change of resistance of metal nanolayers, which could share the same electrical readout principle as the change of resistance of *p-i-n* diodes. This study on thin-metal films as potential ultra-high radiation dosimetry technology, has started by prototyping and testing different type of materials (chromium, aluminum, and copper), with different thicknesses (50, 500, and 1000 nm), and different geometries. Results from the irradiation tests on these Radiation Dependant Resistors (RDR) have shown that no measurable effects were occurring on chromium and aluminum samples, whereas copper samples have shown an increase of resistivity. Such increase was initially explained as result of the increasing displacement damage inside the metal film, directly dependant on the cross section (or interaction probability, calculated with Monte Carlo simulations, to be lower for Cr and Al than for Cu), and on the geometrical characteristic of the RDR (interaction volume).[12] Afterwards, the similarities between the increase of resistivity of Cu RDRs with annealing tests in air at high-temperature (< 150 °C), have suggested an analogy between thermal oxidation, and the radiation triggered Cu corrosion at room temperature.[13]

In this study, to continue our investigation on radiation enhanced oxidation, only copper samples were tested. Furthermore, in order to disentangle the phenomenon of oxidation from the displacement damage, an additional step during the RDRs fabrication was introduced, by sputtering a 300 nm SiO_2 passivation layer through a shadow mask. The RDRs, with and without the passivation layer, that were produced for this experiment, are listed in Table I, with details about their fabrication technique and geometry.

III. METHODS

A. Device microfabrication

All the devices were fabricated at the CMi cleanroom facilities of the Ecole Polytechnique Fédérale de Lausanne (EPFL).[14] A number of wafers were produced, with different copper deposition techniques (evaporated, sputtered), and patterning techniques (lift-off, wet etch, dry etch), in order to test the impact of these fabrication steps to the final RDR performance. The resulting RDR, is a 3 x 3 mm^2 silicon chip with on top a meander shaped metal

TABLE I. List of parameters for each RDR, such as Cu deposition technique, geometrical characteristics (thickness of Cu (t_{cu}) and SiO_2 (t_{SiO_2}), width (W), number of fingers (f), length (L)), and the initial resistance value (R_i) at 21 °C.

	Tag	Cu	t_{cu} [nm]	t_{SiO_2} [nm]	W [μm]	f	L [mm]	R_i [Ω]
PCB1	IC1	Evaporated	550	none	30	25	66.3	79.5
	IC2		590	360	30	25	66.3	76.2
	IC3		540	none	30	19	51.4	64.0
	IC4		600	230	30	25	66.3	76.5
PCB2	IC5	Sputtered	520	none	30	41	109.1	151.2
	IC6		530	350	30	25	66.3	93.0
	IC7		580	none	30	25	66.3	83.1
	IC8		580	290	30	25	66.3	83.2

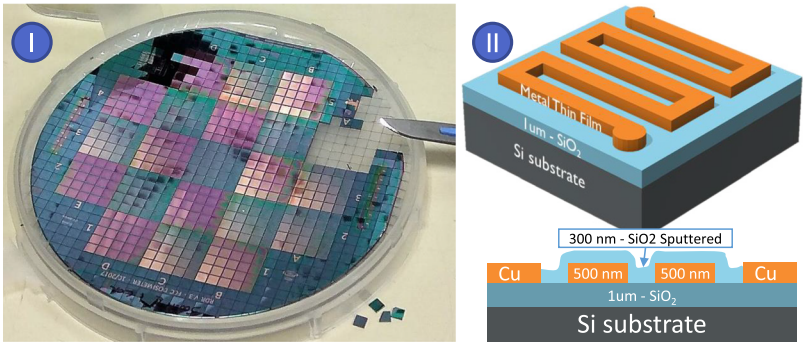

FIG. 1. On the left (I), one of the produced 100 mm wafers, with visible alternated passivation SiO_2 layer (in purple). On the right (II), the 3D model of a Radiation Dependent Resistor and its cross section.

layer, as shown in Fig. 1. For some devices, an extra passivation layer was sputtered through a shadow mask, obtaining the cross section schematized Fig. 1. More details on the fabrication steps can be found in Ref. 13.

B. Testbench and irradiation setup

The samples mounted and wire bonded on PCB sensor carriers (as shown in Fig. 2.I), were connected to the measurement testbench via 30 m long cables running from inside the irradiation bunker to the control room. Any DC measurement error introduced by the long cables, was minimized thanks to a 4-wire readout configuration.

The testbench, was equipped with a Keithley 2410 SMU (Source and Measure Unit) and a Keysight 34970A switch matrix, controlled by a LabVIEW program allowing to address all the devices and the on-board NTC (Negative Temperature Coefficient) sensors. At each readout, every 5 minutes, the resistance values of the RDRs were extrapolated from the slope of a 50-points I-V curves obtained by sweeping the current from 50 µA to 100 µA and measuring the developing voltage. With such readout current, the electric field (E) across the devices was in the order of 50 mV/cm^2, and the current density (J) was kept under 600 A/cm^2, three order of magnitude lower than the reported average electromigration J for copper at room temperature.[15]

The irradiation test has been performed at the IRRAD Proton Facility at CERN,[16] installing the PCBs on the IRRAD7 table as shown in Fig. 2. The samples have been continuously in-beam position, intercepting on average one spill of 5x10^{11} protons every 10 seconds over almost 5 months, reaching a total fluence of 1.2x10^{17} p/cm^2. The dosimetry was performed by aluminum activation-foils located in front of the samples under irradiation. The proton fluence was estimated by counting the ^{22}Na and ^{24}Na activities in the foils, resulting from spallation reactions induced by the 23 GeV proton beam.[17]

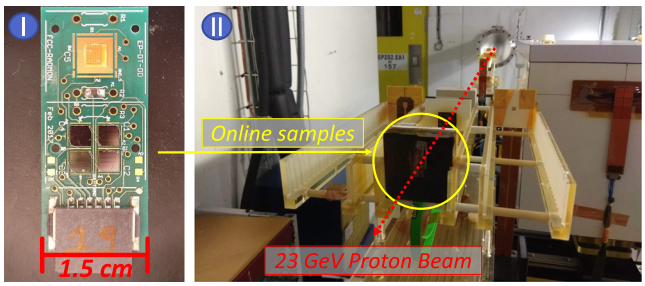

FIG. 2. On the left (I), the PCB sensor carrier mounting multiple Radiation Dependent Resistors and an on-board NTC temperature sensors, on the right (II), a photo of the irradiation table taken inside IRRAD.

C. SEM-FIB analysis

In order to assess the changes on the microstructure, a Zeiss XB540 FIB/SEM was used to perform microscopy on the surface and cross-section of the samples. FIB cross sectional millings were done to reveal cross sections of the Cu layers, and SEM was used to image the samples. The Secondary Electron Secondary Ion (SESI) Detector was used for the imaging. The FIB cross sectional milling was performed across the whole Cu meander in the center of the chip. A 1×3×65 µm^3 Pt barrier was initially deposited on the surface of the sample, at a milling current of 300 pA, in order to protect the sample surface and ensure a sharp cross sectional surface after milling. Coarse milling at 7 nA was then used to remove a 7×7×65 µm^3 region of material. Polishing of the resulting cross sectional surface was performed at 1.5 nA. Imaging was then performed at different magnifications (1.5k, 5k, 20k, and 50k) with an electron high tension varying from 5 kV to 10 kV (the full set of pictures is available in the supplementary material).

D. Temperature characterization

For evaluating the quality of the deposited film in terms of stability and linearity with respect to temperature variation, a temperature characterization was carried out in a dedicated climatic chamber prior irradiation. All the samples have been tested by rising the temperature from 25 °C to 60 °C over 2 hours, followed by a fast ramp up to 100 °C. No shift in the resistance values was measured for any of the devices, resulting in a constant temperature coefficient comparable with results in literature.[18] On another set of devices, an annealing test was performed at 60 °C for a week, and no measurable variation was observed. Similarly, a test at ambient temperature and humidity was carried out for several months, also without signs of further copper oxidation, confirming the stability of these copper films, and the presence of a durable native oxide that prevents the film from further oxidation at temperatures lower than 60 °C.

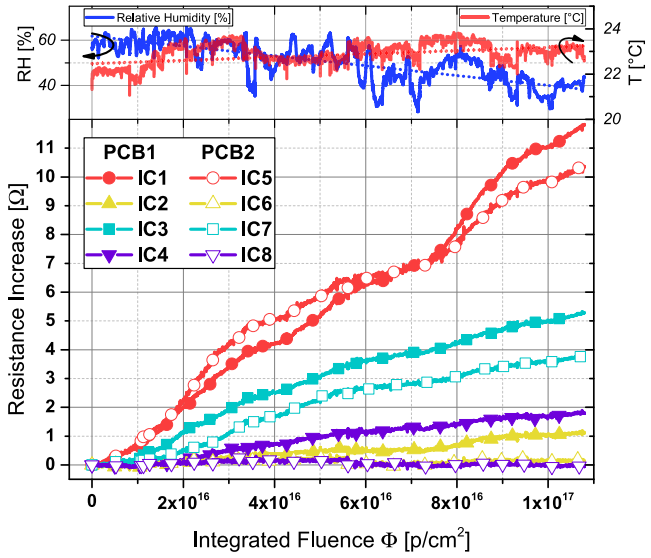

FIG. 3. Resistance variation with increasing integrated proton fluence of all the RDRs on the two PCBs irradiated in IRRAD. The relative humidity (RH) and temperature are shown in the top inset.

IV. RESULTS AND DISCUSSION

A. Electrical measurements

The results from the electrical measurements performed during the proton irradiation experiment in IRRAD are shown in Fig. 3. By comparing the yellow and purple (triangles) curves of the RDRs with a SiO_2 passivation layer, with the non-passivated RDRs in red and cyan (circles and squares), is clear that the SiO_2 layer has a big impact in limiting the increase of resistivity of the Cu layer. In fact, the non-passivated (uncovered) samples have increased up to 12 Ω (+13%) as for the IC5 in Fig. 3, while the SiO_2-passivated (covered) RDRs have not increase at all (IC6 and IC8), or have shown an increase of <2 Ω (+3%) due to partially passivated contact pads as result of misalignment during SiO_2 sputtering. While the integrated fluence can be considered the same for all the RDRs, a wide range of resistance increase can be observed in the non-passivated samples in Fig. 3. Such difference in the sensitivity to radiation of the RDRs can be explained by their different geometrical shape (W, L), copper thickness (t_{Cu}) and deposition technique, as reported in Table I.

In a very high energy proton beam, the interaction probability of a thin metal film is essentially the same for both covered and uncovered RDRs, since the range of 23 GeV protons in Cu of 1 m (or 3 m in SiO_2),[19] is several orders of magnitude larger than the RDR thickness. Therefore, both types of RDRs exhibit the same likelihood of developing defects due to particles interaction, indicating that displacement damage is not the only responsible for the increase of resistivity, and when the Cu layer is encapsulated under a layer of SiO_2, displaced copper atoms do not create any significant variation.

The temperature and relative humidity (RH) were monitored during the whole irradiation, and are reported in the top inset of Fig. 3. It is worth noticing that the increase of resistance of the uncovered RDRs has occurred at temperatures between 20 and 24 °C, much lower than the >100°C required to trigger the standard oxidation. Moreover, even if RH has greatly varied from 60% to 30%, no correlation was found between the rate of resistance increase and RH variation.

B. SEM-FIB inspection

Scanning electron microscopy was used to directly assess the radiation damage in the bulk of the RDRs and, as shown in Fig. 4, compare the FIB milled cross sections of not irradiated RDRs

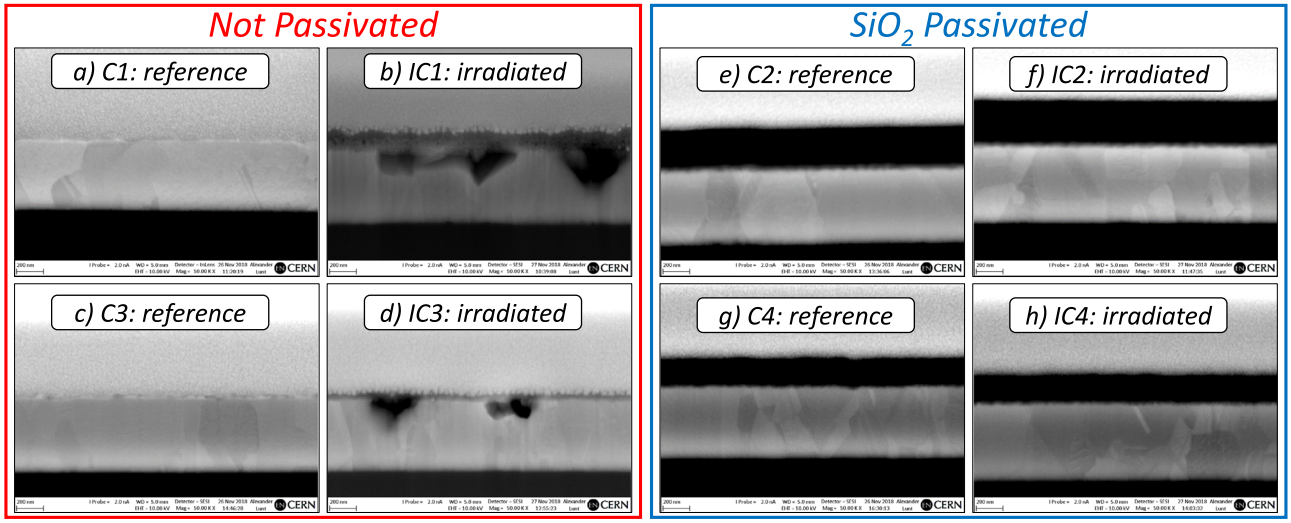

FIG. 4. SEM images at 50k magnification of the cross sections of non-irradiated RDR (a, c, e, g) and irradiated ones (b,d,f,h). In red the non-passivated RDRs and in blue the SiO_2 passivated ones. Black areas are SiO_2, gray areas with grains are Cu, and light gray areas on top are Pt.

(reference samples), both passivated and not, with the irradiated ones. Such analysis has confirmed what has been measured electrically and reported in Fig. 3. The cross sections of the SiO_2 passivated samples (Fig. 4 e, f, g, h) are practically identical for both irradiated and not-irradiated chips. In contrast, the not-passivated samples in Fig. 4b and Fig. 4d, show the presence of large voids, and growth of a uniform oxide layer on the surface (darker contrast on top of Cu), that are not present in the non-irradiated samples Fig. 4a and Fig. 4c.

The formation of voids can be explained by the growth of Cu_2O and CuO oxide layers, which corroded the underlying Cu, and explain the increase of resistivity measured in Fig. 3 for the not-passivated samples. Moreover, the higher increase measured for IC1 with respect to IC3, is compatible with the cross sectional images, where a greater concentration of voids, and a thicker oxide layer, are seen in Fig. 4b with respect to Fig. 4d.

These observations suggest the presence of an oxidation process, occurring in the Cu layers exposed to air, caused by the particle interaction, rather then a classic oxidation caused by a high temperature baking. Such radiation enhanced oxidation process is explored in details in the following sections.

C. Radiation enhanced oxidation

Copper oxidation at different atmospheric conditions is widely documented,[20–23] and the proposed mechanism identifies first the growth of an amorphous cuprous oxide (Cu(I)) layer, at low temperatures and pressures, and then a further oxidation into cupric oxide Cu(II) at higher temperatures:

$$Cu \longrightarrow Cu(I): \qquad 4Cu + O_2 \longrightarrow 2\,Cu_2O \tag{1}$$

$$Cu(I) \longrightarrow Cu(II): \qquad 2Cu_2O + O_2 \longrightarrow 4CuO \tag{2}$$

Also void formation has been documented in studies on copper oxidation,[24,25] and it is associated to the different rate of oxide nucleation due to diverse diffusion rates of oxidants along the grain boundaries, leading to a disordered growth and void creation (also known as Kirkendall voids[26]).

Given the evidences shown in Fig. 3 and Fig. 4, we propose a global behavioural model to connect the standard copper oxidation at different atmospheric conditions, with a radiation triggered oxidation where the energy required to initiate the oxidizing reactions, is given to the lattice by means of particle interactions and not by temperature.

A schematic illustration of the proposed mechanisms involved in the growth of a copper oxide film on a RDR under irradiation, is depicted in Fig. 5, and can be described as:

1. Radiolysis of water at the surface into reactive radicals (such as H_2O_2 and OH^-), due to ionizing energy deposition by incident particles;
2. Electrons are stripped from the oxide along the track of the incident particle;
3. Additional defects and dislocations may occur in the copper layer due to "strong" nuclear reactions (displacement damage "DD"), sputtering and diffusing copper elsewhere;
4. The generated copper ions and electrons diffuse toward the surface along the grain boundaries;
5. Following the equation 1, Cu ions react with oxygen growing new amorphous Cu_2O along grain boundaries creating voids;
6. Further oxidation of Cu_2O into CuO occurs following equation 2.

This proposed global model of radiation enhanced oxidation, is further supported by the presence in literature of similar effects of copper corrosion observed in storage canister for nuclear waste. In this case, due to gamma radiation and heat, radiolysis occurs transforming H_2O molecules into highly reactive species capable to efficiently oxidize copper.[27–29]

D. Analytical model

In this section we propose a model to describe the growth of copper oxide by considering the flux of oxidants along the structure and the oxidizing reactions, not dependent on time, but dominated by the integrated particle fluence. Such assumption can be considered since no oxidation was observed in samples stored at room temperature, while during the same amount of time, samples exposed to radiation have shown a drastic oxidation even if the temperature in the irradiation chamber never exceeded 24 °C. Therefore, we replace time-driven processes to radiation-driven ones, by relating time to the equivalent cumulated particle fluence in 1 hour of irradiation in the IRRAD proton facility:

$$1\ hour = 3.6 \times 10^{12} p/cm^2 \tag{3}$$

As schematized on the right of Fig. 5, a simplified view of the copper oxidation process (similarly to silicon oxidation model by Deal and Groove,[30] and also used for copper in Ref. 23), takes into account two fluxes:

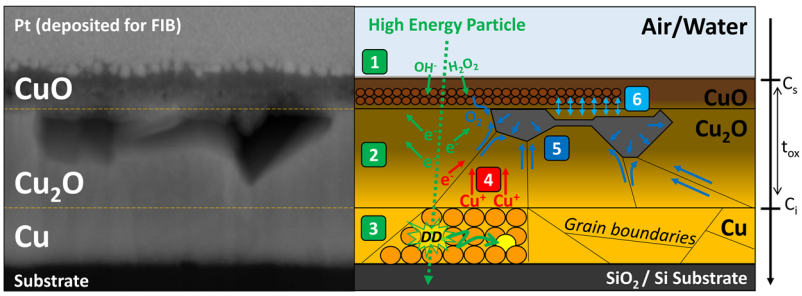

FIG. 5. On the left the SEM picture at 50k magnification of the non-passivated and irradiated IC1. On the right the mechanisms involved in the radiation enhanced oxidation under high energy particle irradiation, as described in Section IV C.

I) F_1: Diffusion through the oxide till the metal-oxide interface proportional to the gradient of oxidants concentration across the oxide ($\frac{dC}{dt_{ox}}$), and to the diffusivity of the oxidants D_{ox}.
(→ *radiation enhancement by steps 1 to 4 in Fig. 5*);

II) F_2: Generation of new atoms of oxide, via chemical reaction at the interface, proportional to the reaction coefficient k_i.
(→ *radiation enhancement by steps 5 and 6 in Fig. 5*);

The equations for each flux can be found in Ref. 30, and are:

$$\begin{aligned} F_1 &= D_{ox}\frac{C_s - C_i}{t_{ox}} \\ F_2 &= k_i C_i \end{aligned} \tag{4}$$

and assuming the steady state condition $F_1 = F_2 = F$ is possible to solve this set of equations obtaining the overall flux of oxidants:

$$F = \frac{D_{ox}C_s}{t_{ox} + \frac{D_{ox}}{k_i}} \tag{5}$$

from which the growth rate of the oxide layer with respect to the particle fluence $\frac{dt_{ox}}{d\phi}$ can be calculated as the ratio between the flux of oxidants F (in Eq. 5), and the total number of available oxidants C_{tot}. Solving the differential equation by integration, with the initial condition of $t_{ox}(\phi{=}0){=}0$, the oxide thickness t_{ox} is expressed as:

$$t_{ox}^2 + At_{ox} - B\phi = 0 \tag{6}$$

where $A = 2D_{ox}/k_i$ and $B = 2D_{ox}C_s/C_{tot}$. Solving this quadratic equation, leads to two solutions depending on the magnitude of Φ:

$$\begin{aligned} &Small\ \Phi \longrightarrow t_{ox} = \frac{B}{A}\Phi \\ &Large\ \Phi \longrightarrow t_{ox} = \sqrt{B\Phi} \end{aligned} \tag{7}$$

revealing two modes of oxidation, an initial linear oxide growth dominated by the reaction coefficient k_i, followed by a parabolic behaviour driven by the diffusion coefficient D_{ox}. The complete derivation of Eq. 7 is provided in the supplementary material.

E. Empirical model

In this section, we propose a simpler linear model to predict the increase of resistance of an RDR when exposed to radiation. The main hypothesis is that the resistance value of an RDR is linearly dependant only on temperature and fluence, and can be then expressed as:

$$R(T,\Phi) = R(\Phi)(1 + \alpha\Delta T) \tag{8}$$

where R(Φ) is the resistance value increasing with fluence, α is the linear temperature coefficient, ΔT is the increase of temperature from 0°C.

R(Φ) can be considered as the parallel resistance between the growing Cu_2O layer and the shrinking Cu layer, as follows:

$$\begin{aligned} &R(\Phi) = R_{ox} \| R_{cu} \quad with: \\ &R_{ox} = \frac{L}{W}\frac{\rho_{ox}}{t_{ox}}; \quad R_{cu} = \frac{L}{W}\frac{\rho_{cu}}{t_{cu}} \end{aligned} \tag{9}$$

where L and W are design parameters of the RDR, ρ_{ox} and t_{ox} are respectively the resistivity and thickness of the copper oxide, while

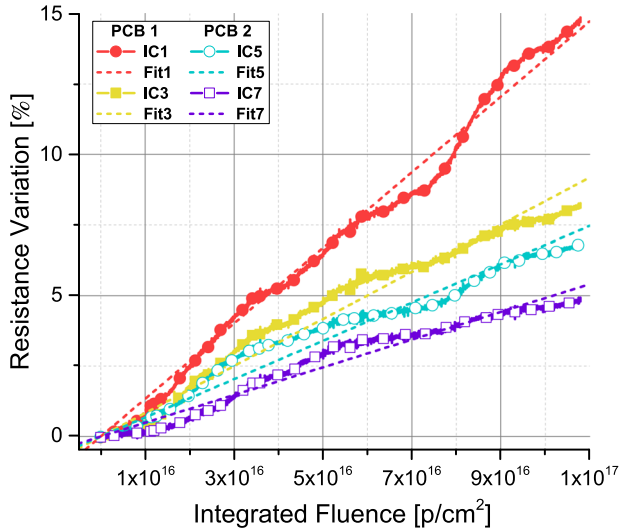

FIG. 6. Extraction of the radiation enhanced oxidation coefficient β (listed in Table II), by linearly fitting the normalized resistance variation $100 \times \frac{R(T,\Phi)-R_T}{R_T}$ with increasing particle fluence (R-Squared >0.99).

ρ_{cu} and t_{cu} are the ones of the copper. By expressing the total thickness t as $t = t_{cu} + 0.3\ t_{ox}$ (see calculations in supplementary material), and simplifying the ratio $(\rho_{cu} - 0.3\rho_{ox})/\rho_{ox} \approx -0.3$ (since $\rho_{ox} \gg \rho_{cu}$[31]), is possible to rewrite $R(\Phi)$ in Eq. 9, and express it as first order Taylor series approximation:

$$R(\Phi) = R_0\frac{1}{1 - 0.3\frac{t_{ox}}{t}} = R_0\sum_{n=0}^{\infty}\left(0.3\frac{t_{ox}}{t}\right)^n \approx R_0\left(1 + 0.3\frac{t_{ox}}{t}\right) \tag{10}$$

where $R_0 = \frac{L}{W}\frac{\rho_{cu}}{t}$ is the RDR resistance at 0°C and Φ = 0, t is the initial thickness, and t_{ox} is the radiation dependent oxide thickness calculated in Eq. 7. By further considering the case of small Φ ($t_{ox} = \frac{B}{A}\Phi$), equation Eq. 10 becomes:

$$R(\Phi) = R_0\left(1 + \frac{0.3}{t}\frac{B}{A}\Phi\right) = R_0(1 + \beta\Phi) \tag{11}$$

with $\beta = \frac{0.3}{t}\frac{B}{A}$ which is the radiation enhanced oxidation coefficient. As shown in Fig. 6, β can be extracted by a linear fit of the temperature-corrected resistance variation during irradiation, and by finally rewriting Eq. 8, an estimate of the integrated fluence Φ can be obtained as:

TABLE II. Extracted temperature coefficients α and radiation coefficients β, for the different uncovered Cu RDR under test.

	Tag	R_0 [Ω]	α [1/°C]	β [cm²/p]
PCB1	IC1	73.36	0.00391	$1.34\text{x}10^{-16}$
	IC3	59.28	0.00377	$8.35\text{x}10^{-17}$
PCB2	IC5	139.93	0.00379	$6.79\text{x}10^{-17}$
	IC7	77.41	0.00361	$4.91\text{x}10^{-17}$

$$\Phi = \left(\frac{R(T,\Phi)}{R_0(1+\alpha\Delta T)} - 1\right)\frac{1}{\beta} \quad (12)$$

where $R(T, \Phi)$ is the experimentally measured RDR's resistance, $R_0(1 + \alpha\Delta T)$ is the temperature dependent resistance R_T. The extracted values of R_0, α, and β, for the four not-passivated RDRs, are listed in Table II. The complete derivation of Eq. 12 is provided in the supplementary material.

V. CONCLUSIONS AND OUTLOOK

In this paper, we have shown and discussed the results from the irradiation tests performed on several devices made of copper. A strong correlation was observed, between resistance variations of the nanometer thick copper layer, and the increasing particle fluence. SEM imaging of the cross sections has further confirmed such resistance variation, revealing areas with grown copper oxides (Cu_2O and CuO) and large voids. We explained such resistance increase by a corrosion of the copper layer as result of chemical and nuclear processes induced by the interaction with energetic particles. We suggested relating conventional copper oxidation at high temperature to a radiation enhanced oxidation at room temperature. We then suggested a simple model that accounts for a radiation enhanced diffusion rate of oxidants across the forming oxide layer (due to water radiolysis at the surface and electron emission in the oxide), as well as a radiation enhanced chemical reaction at the interface (due to the induced displacement damage in the copper lattice). We finally proposed a linear model to account for resistance variation of copper films due to temperature shifts (α), and increasing integrated particle fluence (β), which first applicability is foreseen in the field of dosimetry in form of Radiation Dependent Resistors.

An additional refinement to this model is to consider also the effects of varying air-humidity, which as reported in literature, can increase the oxidation rate by +50% when oxidizing at 30% RH instead of 0% RH.[32] Such dependence on the relative humidity could be taken into account by including a logarithmic term into the radiation enhanced oxidation coefficient β in Eq. 8. Moreover, to better understand the different impacts of the geometrical parameters to the β coefficient, dedicated test structures will be produced and tested. The chemical reactions in the proposed empirical model strongly depend on the quality of the deposited copper (size and shape of the Cu grains determine the oxidants diffusivity), so the larger the surface ($W \times L$) the less impact will small defects in the Cu layer have. Similarly, the extent of nuclear interactions are driven by the interaction volume (more material means greater probability for an incident particle to displace an atom), so thicker structures would be more prone to displacement damage. Such geometrical modifications will overall vary the amount of copper oxide with respect to the initial copper (the ratio t_{ox}/t_{cu}), thus trimming the range of resistance increase. Furthermore, by patterning the protective SiO_2-passivation area, leaving uncovered only some sections of the device, the RDR can be engineered to target the sensitivity range of the specific application.

In summary, in this paper, the underlying effects responsible for the resistivity increase of irradiated copper thin films have been studied in detail, and a model of radiation enhanced oxidation matching the experimental data has been proposed. A first application for a predictable radiation-enhanced oxidation is to related Such effects are at the base of the copper Radiation Dependent Resistors have shown to be a promising candidate technology for extending the detection capability of current silicon-based dosimeters. Further development of the Radiation Dependent Resistors will allow developing sensors compatible with very high radiation levels in applications such as nuclear and fusion energy, as well as matching the detection requirements in high energy physics experiments, such as the extreme radiation environment expected in the Future Circular Collider.

SUPPLEMENTARY MATERIAL

See supplementary material for the complete derivation of the analytical and the empirical models, as well as the complete set of SEM pictures.

ACKNOWLEDGMENTS

The authors would like to thank A. Lunt, A.T. Perez, and E.G. Tabares from CERN-EN-MME for performing the SEM-FIB imaging. We also wish to express our gratitude to M. Moll and M. Capeans from CERN-EP and J. Bronuzzi and C. Rossi from EPFL-EDLAB for their help and support. This work was funded by the CERN Future Circular Collider, Special Technologies, Radiation Hardness Assurance, Work Package 11.

REFERENCES

[1] R. Flukiger and T. Spina, "The behaviour of copper in view of radiation damage in the LHC luminosity upgrade," in Workshop on Accelerator Magnet, Superconductor, Design and Optimization, CERN, Geneva, Switzerland, **76–82**. 7 p (2014).
[2] L. K. Mansur, "Theory and experimental background on dimensional changes in irradiated alloys," Journal of Nuclear Materials **216**, 97–123 (1994).
[3] J. O. Stiegler and L. K. Mansur, "Radiation effects in structural materials," Annual Review of Materials Science **9**, 405–454 (1979).
[4] R. L. Chaplin and R. R. Coltman, "Defects and transmutations in reactor-irradiated copper," Journal of Nuclear Materials **108-109**, 175–182 (1982).
[5] NASA, "Nuclear and space radiation effects on materials, NASA Space Vehicle Design Criteria- (Structures)," 44 (1970).
[6] M. Robinson and F. J. Young, "Fundamental aspects of radiation damage in metals," in Proceedings of an international conference, Gatlinburg, Tennessee, October 6–10, 1975.
[7] S. J. Zinkle, *Comprehensive Nuclear Materials*, 1st ed. (Elsevier Inc., 2012), Vol. 1, pp. 65–98.
[8] A. Y. Dunn, "Radiation damage accumulation and associated mechanical hardening in thin films and bulk materials," 303 (2016).
[9] F. Ravotti, L. Dusseau, M. Moll, and E. Tsesmelis, "Development and Characterisation of radiation monitoring sensors for the high energy physics experiments of the CERN LHC accelerator," (2006), presented on 17 Nov 2006.
[10] M. Benedikt, M. Capeans Garrido, F. Cerutti, B. Goddard, J. Gutleber, J. M. Jimenez, M. Mangano, V. Mertens, J. A. Osborne, T. Otto, J. Poole, W. Riegler, D. Schulte, L. J. Tavian, D. Tommasini, and F. Zimmermann, "Future Circular Collider," Tech. Rep. CERN-ACC-2018-0058 (CERN, Geneva, 2018) submitted for publication to Eur. Phys. J. ST.
[11] M. I. Besana, F. Cerutti, A. Ferrari, W. Riegler, and V. Vlachoudis, "Evaluation of the radiation field in the future circular collider detector," Physical Review Accelerators and Beams **19**, 111004 (2016).
[12] G. Gorine, G. Pezzullo, I. Mandic, A. Jazbec, L. Snoj, M. Capeans, M. Moll, D. Bouvet, F. Ravotti, and J. M. Sallese, "Ultrahigh fluence radiation monitoring technology for the future circular collider at CERN," IEEE Transactions on Nuclear Science **65**, 1583–1590 (2018).

[13]G. Gorine, G. Pezzullo, M. Moll, M. Capeans, K. Väyrynen, M. Ritala, D. Bouvet, F. Ravotti, and J.-M. Sallese, "Metal Thin-film dosimetry technology for the ultra-high particle fluence environment of the future circular collider at CERN," RAD Association Journal **3**, 172–177 (2019).
[14] "Cmi - center of micronanotechnology - epfl," https://cmi.epfl.ch/, accessed: 2019-03-15.
[15]P. C. Wang and R. G. Filippi, "Electromigration threshold in copper interconnects," Applied Physics Letters **78**, 3598–3600 (2001).
[16]B. Gkotse, M. Brugger, P. Carbonez, S. Danzeca, A. Fabich, R. G. Alia, M. Glaser, G. Gorine, M. Jaekel, I. Mateu, G. Pezzullo, F. Pozzi, F. Ravotti, M. Silari, and M. Tali, "Irradiation Facilities at CERN," in *RADECS 2017* (2017).
[17]A. Curioni, R. Froeschl, M. Glaser, E. Iliopoulou, F. La Torre, F. Pozzi, F. Ravotti, and M. Silari, "Single- and multi-foils ^{27}Al(p,3pn)^{24}Na activation technique for monitoring the intensity of high-energy beams," Nuclear Instruments and Methods in Physics Research Section A: Accelerators, Spectrometers, Detectors and Associated Equipment **858**, 101–105 (2017).
[18]J. Dellinger, "The temperature coefficient of resistance of copper," Journal of the Franklin Institute **170**, 213–216 (1910).
[19]M. Berger, J. Coursey, and M. Zucker, "Stopping-power and range tables for electrons, protons, and helium ions," (2000).
[20]P. K. Krishnamoorthy and S. C. Sircar, "Formation of very thin oxide films on copper: Kinetics and mechanism," Oxidation of Metals **2**, 349–360 (1970).
[21]Y. Zhu, K. Mimura, and M. Isshiki, "Oxidation mechanism of Cu_2O to CuO at 600-1050 °C," Oxidation of Metals **62**, 207–222 (2004).
[22]C. Gattinoni and A. Michaelides, "Atomistic details of oxide surfaces and surface oxidation: the example of copper and its oxides," Surface Science Reports **70**, 424–447 (2015), arXiv:1508.01005.
[23]S. Choudhary, J. V. Sarma, S. Pande, S. Ababou-Girard, P. Turban, B. Lepine, and S. Gangopadhyay, "Oxidation mechanism of thin Cu films: A gateway towards the formation of single oxide phase," AIP Advances **8** (2018).
[24]Z. Han, L. Lu, H. W. Zhang, Z. Q. Yang, F. H. Wang, and K. Lu, "Comparison of the oxidation behavior of nanocrystalline and coarse-grain copper," Oxidation of Metals **63**, 261–275 (2005).
[25]S. Samal, "High-Temperature Oxidation of Metals," in *High Temperature Corrosion*, Vol. 12 (InTech, 2016) pp. 11–17, 9809069v1 [arXiv:gr-qc].
[26]C. J. Love, J. D. Smith, Y. Cui, and K. K. Varanasi, "Size-dependent thermal oxidation of copper: Single-step synthesis of hierarchical nanostructures," Nanoscale **3**, 4972–4976 (2011).
[27]S. Le Caër, "Water radiolysis: Influence of oxide surfaces on H_2 production under ionizing radiation," Water **3**, 235–253 (2011).
[28]T. Björkbacka, S. Hosseinpour, M. Johnson, C. Leygraf, and M. Jonsson, "Radiation induced corrosion of copper for spent nuclear fuel storage," Radiation Physics and Chemistry **92**, 80–86 (2013).
[29]B. Ibrahim, D. Zagidulin, M. Behazin, S. Ramamurthy, J. C. Wren, and D. W. Shoesmith, "The corrosion of copper in irradiated and unirradiated humid air," Corrosion Science **141**, 53–62 (2018).
[30]B. E. Deal and A. S. Grove, "General relationship for the thermal oxidation of silicon," Journal of Applied Physics **36**, 3770–3778 (1965).
[31]L. De Los Santos Valladares, D. H. Salinas, A. B. Dominguez, D. A. Najarro, S. I. Khondaker, T. Mitrelias, C. H. Barnes, J. A. Aguiar, and Y. Majima, "Crystallization and electrical resistivity of Cu_2O and CuO obtained by thermal oxidation of Cu thin films on SiO2/Si substrates," Thin Solid Films **520**, 6368–6374 (2012).
[32]Z. Feng, C. R. Marks, and A. Barkatt, "Oxidation-rate excursions during the oxidation of copper in gaseous environments at moderate temperatures," Oxidation of Metals **60**, 393–408 (2003).